Sigma Journal of Engineering and Natural Sciences
Web page info: https://sigma.yildiz.edu.tr
DOI: 10.14744/sigma.2025.1911

Research Article

Effect of pier-collar system on flow characteristics of composite hydraulic structure

Rafi Mohammed QASIM[1], Khalid AL-ASADI[2], Ihsan Abdulkareem ABDULHUSSEIN[1,*], Qusay Abdulrazzaq MAATOOQ[1]

[1]*Southern Technical University, Basrah Engineering Technical College, Basrah, 15425650, Iraq*
[2]*Department of Civil and Architectural Engineering and Mechanics, University of Arizona, 85721, USA*

ARTICLE INFO

Article history
Received: 15 May 2024
Revised: 18 July 2024
Accepted: 17 October 2024

Keywords:
Collar; Composite Hydraulic Structure; Flume; Gate; Pier; Weir

ABSTRACT

The weir-gate compound structure hydraulic characteristics and the hydraulic behavior of the pier mounted by a collar at the base are investigated experimentally. This investigation refers to the fluid-structure interference and, on the other hand, represent the interference among two different structures installed inside the channel. So both structures have a direct influence on the flow features between them. The main target of this work, reveal how the pier-collar system share in raise water depth and how share in change the hydraulic features of weir-gate. The study adopted different weir shapes with an ellipse gate, as well as different sizes of the pier and the collar, to perform the experiments. From the experiments, it was found that the pier size, collar size, and weir shape produced a nonlinear water surface profile at the composite hydraulic structure downstream region. The drag force, static force, and moment that are grown at the pier base are more influenced by the alteration in flow velocity and flow depth that occurs owing to the presence of the pier and the collar. More specifically, the change in the flow velocity and the flow depth due to the presence of the pier and the collar will be reflected directly in the obtained values of the Froude number and Reynolds number. Overall, the collar has a moderate effect on the hydraulic characteristics as compared with the pier. The result shows a discharge coefficient has a direct proportional with actual discharge. The quantitative result which appears from this study the downstream water depth and actual flow rate obey and satisfy confident level equal to and greater than 95%.

Cite this article as: Qasim RM, Al-Asadi K, Abdulhussein IA, Maatooq QA. Effect of pier-collar system on flow characteristics of composite hydraulic structure. Sigma J Eng Nat Sci 2025;43(6):2066–2083.

INTRODUCTION

The weir-gate hydraulic structure is characterized by an absolutely necessary quality that gives attention to managing the water flow either by the use of an open or artificial channel, which can not make any clash in the channel hydraulic characteristics with any hydraulic structure, which is found in the channel. In addition,

***Corresponding author.**
*E-mail address: drengihssan@stu.edu.iq

This paper was recommended for publication in revised form by Editor-in-Chief Ahmet Selim Dalkilic

the structure of weir-gate is used in gauging the control and trying to change any direction flow without showing any condition of not having enough deficit. To tackle this issue, the existence of the weir-gate structure in a channel alone has been dealt with by several studies, whereas little work has been done on the effect of the difficulty experienced on the structure of weir-gate or the interplay between the structure of weir-gate and other structures. These studies are outlined as follows: Qasim et al. [1] performed many experiments on checking the hydraulic patterns of the compound hydraulic structure in order to compare between the state of free flow, that prevailed with no appearance of any obstacle at the downstream of the composite structure, and the state of submerged flow, which is found as a result of existing the obstacle at the downstream of the composite structure. Besides, it is noted that this investigation briefly concentrated on the geometric and hydraulic variables. Abdulhussein et al. [2] tested the composite discharge structure activity owing to the finding of the prevailing longitudinal obstacle. Their study dealt with two parts: the first was based on the experimental work, whereas the second discussed the statistical analysis and the results arrived at from the experiment work done in the first part. Here, the effect of cross-sectional area of the obstacle has been taken into consideration. In this study, the obstacle length is taken into consideration. Referring to this aspect, the longitudinal obstacle shows that there is a significant effect on the hydraulic quantities that are typical for the structure of composite discharge. Also, Abdulhussein et al. [3] executed an experimental work to tackle the interaction found among the hydraulic variables, which showed that there is a strong central influence on the discharge structure work and the obstacles dimensions, which is found at the downstream of the discharge flow. In addition to this, the optimal dimensions of the obstacle have been measured by employing optimization analysis. Referring to Qasim et al.'s studies were done in [4-6], the alteration of the flow properties and the patterns obtained owing to the interaction found among the combined hydraulic structure and the emerging obstacle were taken into consideration. Abdulhussein et al. [7] arrived at a general equation that was taken from the experimental work done to expect the flow rate that passes through the discharge structure. This equation has been derived from the free-flow case. To get reliable data, different shapes of gates and weirs have been adopted. Qasim et al. [8], in an experimental study, examined the effect of the discharge structure's inclination angle on its hydraulic use. In this respect, the inclination angle values are also examined, and several hydraulic factors affecting the discharge structure are studied too. Abdulhussein et al. [9] examined how the weir crest thickness is influenced by the composite hydraulic structure. Qasim et al. [10] gave an evaluation of the main and secondary factors that created influence on the way about the response of the composite hydraulic structure, which shows that there is a contraction between the discharge coefficient, and hydraulic and geometrical factors. Qasim et al. [11] experimentally checked the bed flume contraction's effect on the discharge coefficient for the combined hydraulic structure, as well as they made a comparison between the obtained results or values and the values of the discharge coefficient in relation to the bed with no contraction. Qasim et al. [12-14] made an experiment to examine how the hydraulic structure responds to the combined hydraulic structure. They also focused on investigating the hydraulic and geometrical variables; it tried to find out the difference between these variables. To maintain this type of investigation, the different shapes of weirs and gates featured by the regular and irregular sections are also depended. Qasim et al. [15] studied experimentally the impact of the bed flume discordance on the weir-gate structure. Several variables are adopted in this study, considering different configurations of bed flume discordance. Gharehbaghi et al. [16] used three different models to predict the streamlined weir discharge coefficient; these models are gene expression program methods, intelligent optimization models, and machine learning methods. Based on the scatter plot and statistical metrics, the gene expression program has estimated the value of the discharge coefficient with high accuracy and performance. Li et al. [17] estimated the discharge coefficient of the side semi-circular weir by three optimization algorithms and a support vector machine. It has been shown that the genetic algorithm and support vector machine give accuracy of prediction. Iqbal and Ghani [18] predicted the flow rate capacity of piano key weirs relied on different geometrical variables. Artificial neural networks have been employed to obtain the flow rate. In addition to testing the activity of artificial neural networks, support vector analysis, nonlinear regression, and adaptive neuro-fuzzy interference systems are applied to check the performance of artificial neural networks. Kartal and Emiroglu [19] studied experimentally the flow features of the side weir-gate structure. 650 tests are carried out to estimate the flow features of the weir gate under subcritical flow. Nouri and Hemmati [20] dealt with the discharge coefficient of the weir-gate structure. The Flow-3D numerical model, artificial intelligence models, and regression equation are adopted to compute the discharge coefficient. In order to explore the influence of the pier's existence on the hydraulic characteristics of the composite hydraulic structure, a series of experimental runs are made in the laboratory. Here, the pier is mounted by a collar. The work gives a noticeable realization about the impact of geometrical variables of any obstacle like a pier-collar system on the hydraulic variables of weir-gate structure depending on the different variables. These variables are built based on different pier size, collar size, collar thickness, weir shape, gate dimension, and different downstream distance. Moreover, the effect of downstream water raises on the drag force that has been developed

on the pier and collar is investigated, and the variation in hydrostatic pressure around the pier-collar system is estimated. The unique contribution of the study is based on giving a good vision about the obstacle's existence (in this paper, a pier mounted by a collar is adopted), which led to a rise in water level downstream of the weir gate. It also gives a vision about the variation in the flow velocity owing to the existence of the obstacle, which in turn has a direct effect on the momentum alteration. Therefore, we deal with the subject in order to summarize the contribution on the hydraulic features of weir-gate structures, which are broadly used in water structure work.

FLUID MECHANICS CONCEPTT

The total actual discharge that passes the composite weir-gate hydraulic structure can be determined from:

$$Q_{act} = C_d \cdot (Q_{w,theo} + Q_{g,theo}) \quad (1)$$

where Q_{act}, is the total actual discharge through the composite structure (m^3/sec); $Q_{w,theo}$ and $Q_{g,theo}$ are the theoretical discharges through the weir and gate structures, respectively (m^3/sec); C_d is coefficient of discharge for the composite structure (dimensionless).

Different compound weir-gate shapes were used in this study as indicated below.

Triangular weir – Ellipse gate

Theoretical discharges that pass the triangular weir and ellipse gate can be calculated using equations (2) and (3), respectively [21].

$$Q_{w,theo} = \frac{8}{15}\sqrt{2g}\ \tan\frac{\emptyset}{2}\ h_u^{5/2} \quad (2)$$

$$Q_{g,theo} = \sqrt{2gH}\,A_g \quad (3)$$

According to eq. (1), the total actual discharge that passes through the composite triangular weir-ellipse gate hydraulic structure is:

$$Q_{act} = C_d \left[\frac{8}{15}\sqrt{2g}\ \tan\frac{\emptyset}{2}\ h_u^{5/2} + \sqrt{2gH}\,A_g\right] \quad (4)$$

Rectangular weir – Ellipse gate

Theoretical discharge that passes rectangular weir can be calculated using equations (5) [21].

$$Q_{w,theo} = \frac{2}{3}\sqrt{2g}\ b\ h_u^{3/2} \quad (5)$$

According to eq. (1), the total actual discharge that passes through the composite rectangular weir-ellipse gate hydraulic structure is:

$$Q_{act} = C_d \left[\frac{2}{3}\sqrt{2g}\ b\ h_u^{3/2} + \sqrt{2gH}\,A_g\right] \quad (6)$$

Parabolic weir – Ellipse gates

Theoretical discharge that passes parabolic weir can be calculated using equations (7) [22].

$$Q_{w,theo} = \frac{\pi}{2}\sqrt{f\,g}\cdot h_u^2 \quad (7)$$

According to eq. (1), the total actual discharge that passes through the composite parabolic weir-ellipse gate hydraulic structure is:

$$Q_{act} = C_d \left[\frac{\pi}{2}\sqrt{f\,g}\cdot h_u^2 + \sqrt{2\,g\,H}\ A_g\right] \quad (8)$$

For free flow condition

$$H = d + y + h_u \quad (9)$$

For submerged flow condition

$$H = d + y + h_u - h_d \quad (10)$$

where g is the gravitational acceleration; ϕ is weir angle; H and h_d refer to flow depths at the upstream and downstream of the weir-gate structure, respectively; h_u represents flow depth above weir crest; A_g is gate cross sectional area; y is vertical distance between weir and gate; d is gate opening height; f is focal distance; b is rectangular weir width.

The Reynolds number (R_n) and Froude number (F_r) are calculated by using the following equations (18 and 19) [23]:

$$R_n = \frac{Vh}{\nu} \quad (11)$$

$$F_r = \frac{V}{\sqrt{gh}} \quad (12)$$

Where V is flow velocity, h is flow depth, and ν is the kinematic viscosity of water.

The drag force (F_D) exerted by the pier or collar is calculated using the following equation (19).

$$F_D = \frac{1}{2}\rho\, C_D V^2 Ap \quad (13)$$

where ρ is water density, Ap is a pier or collar projected area, and C_D is drag coefficient.

The C_D value for a cylindrical collar is equal to 1.2 (19), whereas the C_D value for a cylindrical pier can be calculated using the following equation, Cheng, [24] :

$$C_D = 11\,R_n^{-0.75} + 0.9\left[1-\exp\left(-\frac{1000}{R_n}\right)\right] + 1.2\left[1-\exp\left(-\left(\frac{R_n}{4500}\right)^{0.7}\right)\right] \quad (14)$$

Equation (15) was used to calculate the hydrostatic force (F_p) resulting from the hydrostatic pressure surrounding the pier:

$$F_P = \frac{1}{2}\,\rho\, g\, h^2 D_p \quad (15)$$

where D_p is pier diameter.

EXPERIMENTAL SETUP

Several experimental tests have been executed in a rectangular glass flume at the hydraulics laboratory of Basrah Technical Engineering College. The flume is 200 cm long, 7.5cm wide (B), and 15cm deep with a horizontal bed. The flow rate (discharge) through the flume was controlled by a control valve installed at the flume inlet. The depth of the water is determined by a scale fixed to the flume wall, while the volume method is utilized to measure the total actual discharge. The hydraulic structures of different shapes (Fig. 1) were installed at a distance of 80 cm from the beginning of the flume. The hydraulic structures' models were made from a wood sheet 5 mm thick and beveled along all the edges at 45^0 with sharp edges of thickness 1mm, Qasim et al. [12]. Table 1 shows the selected dimensions of the composite hydraulic structures' models. Cylindrical piers of different ($D_{p)}$ values (1cm, 2cm, 3cm, 4cm, and 5cm) mounted by collars of different diameter (D_r) values (4cm, 5cm, and 6cm) and different depth (te) values (0.5cm and 1cm) were installed at the flume and placed at a distance of 40cm downstream of the composite structure. (Fig. 2). Piers and collars models were made from wood material.

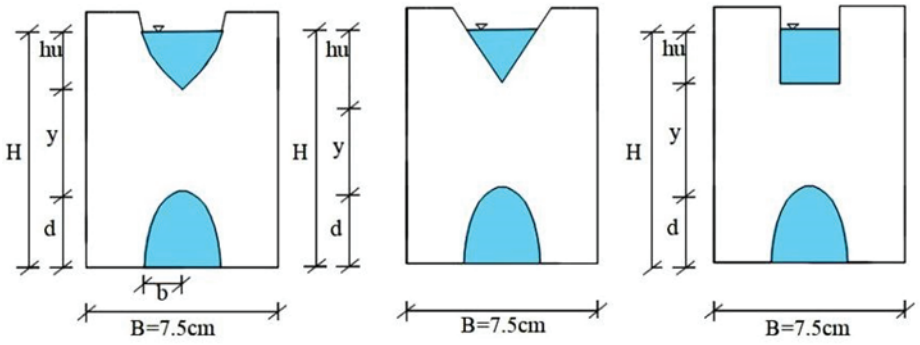

Figure 1. Shapes and dimensions of composite hydraulic structures.

Table 1. Tested model shapes and dimensions

Model	hu (cm)	y (cm)	d (cm)	H (cm)	b (cm)	Aw (cm^2)	Ag (cm^2)	Weir shape	Gate shape
1	3	4.5	2.5	10	1.25	6.93	4.9087	Rectangular	Ellipse
2	2	4.5	2.5	9	1.25	4.62	4.9087		
3	1	4.5	2.5	8	1.25	2.31	4.9087		
4	3	4.0	3.0	10	1.50	6.93	7.0686		
5	2	4.0	3.0	9	1.50	4.62	7.0686		
6	1	4.0	3.0	8	1.50	2.31	7.0686		
7	3	4.5	2.5	10	1.25	6.92	4.9087	Parabolic	Ellipse
8	2	4.5	2.5	9	1.25	3.77	4.9087		
9	1	4.5	2.5	8	1.25	1.34	4.9087		
10	3	4.0	3.0	10	1.50	6.92	7.0686		
11	2	4.0	3.0	9	1.50	3.77	7.0686		
12	1	4.0	3.0	8	1.50	1.34	7.0686		
13	4	3.5	2.5	10	1.25	6.92	4.9087	Triangular	Ellipse
14	3	3.5	2.5	9	1.25	3.89	4.9087		
15	2	3.5	2.5	8	1.25	1.73	4.9087		
16	1	3.5	2.5	7	1.25	0.43	4.9087		
17	4	3.0	3.0	10	1.50	6.92	7.0686		
18	3	3.0	3.0	9	1.50	3.89	7.0686		
19	2	3.0	3.0	8	1.50	1.73	7.0686		
20	1	3.0	3.0	7	1.50	0.43	7.0686		

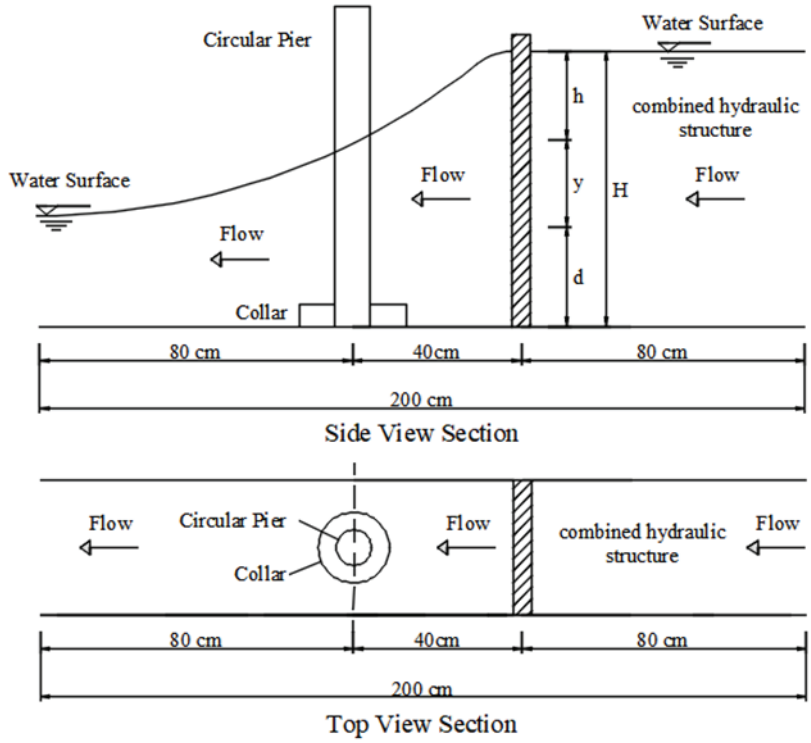

Figure 2. Whole components of hydraulic regime.

An Uncertainty in the Measured Amount

Reliability is the need of every scientific product. The failure of an engineered product is a fixed characteristic or is related to its production. Engineering systems play an important role in making or inventing better reliable products. Uncertainty is the most useful function for analyzing prediction age and reliability. This function can provide the probability of successful operation of the product for up to a certain time without a single failure. Every time, it is not possible to measure the various parameters of the system exactly due to the uncertainty or ambiguity present in their limits. In cases of lack of precision, it is reasonable to use fuzzy parameters rather than exact parameters (values) [25-27]. It is very common for error in parameters to be due to machine error, experimentation, or personal decision. Theories and concepts of uncertainty have been developed and worked on by several researchers, such as; Chandola et al., Sharma et al, Negero et al., Hogeme et al., and Younus et al. [28-32].

Uncertainty is a positive parameter that describes the range of values associated with a measure (the measured quantity). The following equation can be used to express the potential inaccuracies that may arise when measuring a quantity:

$$u_x = \sqrt{S_x^2 + b_x^2} \tag{16}$$

where S_x accounts for the random errors, while the term b_x represents the systematic errors, and u_x is termed the standard uncertainty in x. The sample standard deviation can be used to get the S_x value:

$$S_x = \left\{\frac{1}{N-1}\sum_{i=1}^{N}(x_i - \bar{x})^2\right\}^{1/2} \tag{17}$$

The following equation is used to estimate the uncertainty of a mean value ($U_{\bar{x}}$), which is calculated from a series of N measurements obtained with the same instrument:

$$U_{\bar{x}} = \sqrt{S_{\bar{x}}^2 + b_{\bar{x}}^2} \tag{18}$$

where $S_{\bar{x}}$ is the standard uncertainty of the mean, which is equal to ($=S_x/\sqrt{N}$) while the variable $b_{\bar{x}}$ is the standard deviation linked to systematic errors. It turns out that $b_{\bar{x}} = b_x$.

The standard uncertainty can be multiplied by a coverage factor (k) to determine the extended uncertainty. For example, uncertainty in x can be solved using the following equation:

$$U_{\bar{x}} = k.u_{\bar{x}} = k.\sqrt{S_{\bar{x}}^2 + b_{\bar{x}}^2} \quad (P\%) \tag{19}$$

The k value depends on numerous factors, such as the number of data points and level of confidence P. A P value of 0.95 and 0.99 can be obtained by adjusting the k factor value to equal 2 and 2.6, respectively [33-34].

The uncertainty of a variable indicates what interval the measurement's actual value is most likely to fall inside. The following formats are feasible for the uncertainty interval:

Uncertainty interval=middle value±uncertainty (*P*%) (20)

We want to estimate the uncertainty interval for a population's mean (μ). The uncertainty interval for the true mean value is defined as:

$$\mu = \bar{x} \pm U_{\bar{x}} \quad (P\,\%) \tag{21}$$

MATERIALS AND METHODS

The method used to do this study consists of three parts; these parts are experimental work, hydraulic analysis, and statistical analysis. The experimental works include the following activities: preparing the channel, pump operation to feed the required water quantity, monitoring the water depth over the weir, and finally measuring the flow rate and the flow depth. The hydraulic analysis includes giving a suitable clarification for the relation between hydraulic variables and geometrical variables or relation among the hydraulic variables and the statistical analysis based on analysis of the results of the measured flow rate and the downstream water depth by uncertainty analysis to achieve the required confidence.

RESULTS AND DISCUSSION

As indicated earlier, the main purpose of this study is to investigate the effect of the pier-collar system on the hydraulic characteristics of the composite weir-gate structure. All experimental runs conducted in this study show submerged flow conditions (eq. 10) where the h_d values are greater than the gate height.

Figure 3 shows the variation of the h_d values along the flume reach downstream of the rectangular weir-ellipse gate structure with a pier-collar system of different D_p values, D_r values, and te values of 5cm and 0.5cm, respectively. It can be seen from this figure that the h_d profile is almost nonlinear for all pier diameters, and the h_d values at the upstream region of the pier-collar system are higher than those at the downstream region of the system. This is because of the existence of the pier, which acts as an obstacle to the flowing water.

In Figure 4, the h_d values were sketched along the flume reach downstream of the rectangular weir-ellipse gate structure with a pier-collar system of D_p value 3cm, different D_r values, and te value 0.5cm. It is obvious from this figure that the D_r values have a great effect on the h_d values at the upstream region of the pier-collar system, whereas this effect becomes less noticeable at the downstream region of the system, where there is a slight change in the h_d values. At every section along the upstream region of the pier-collar system, the h_d values increase with increasing D_r values.

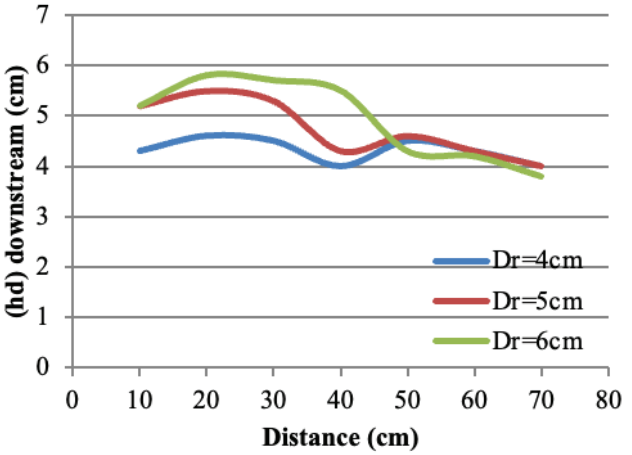

Figure 4. The variation of h_d values along the downstream distance of the rectangular weir-ellipse gate structure for different D_r values (D_p= 3cm, te= 0.5cm).

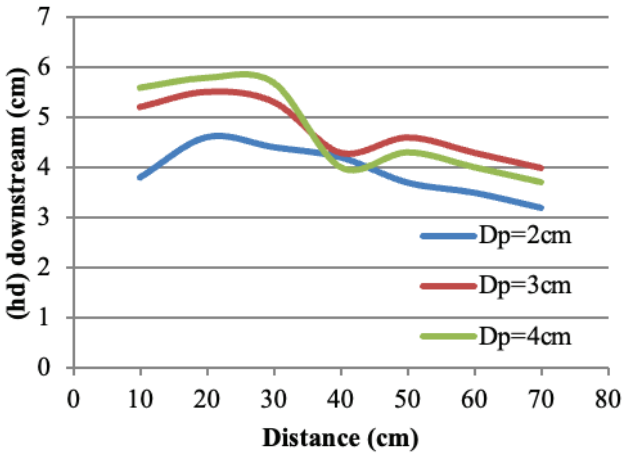

Figure 3. The variation of h_d values along the downstream distance of the rectangular weir-ellipse gate structure for different D_p values and D_r= 5cm and te= 0.5cm.

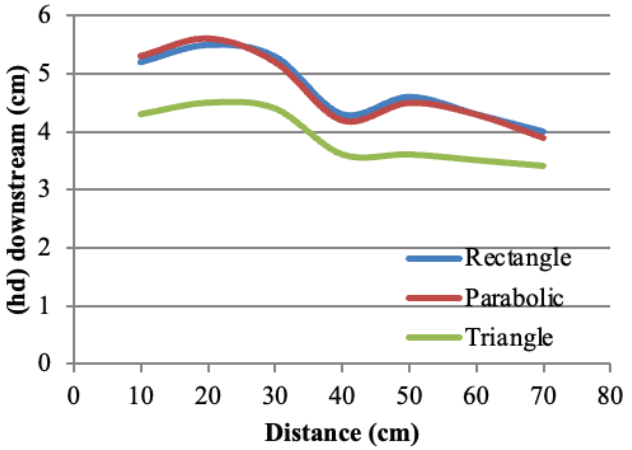

Figure 5. The variation of h_d values along the downstream distance of the composite structure of different weir shapes (D_p= 3cm, D_r=5cm, te= 0.5cm).

This means that the collar also works as an obstacle, and its effect increases with increasing diameter.

Figure 5 shows the variation of the h_d values along the flume reach downstream of the composite hydraulic structure of different weir shapes with pier-collar systems of D_p, D_r, and te equal to 3cm, 5cm, and 0.5cm, respectively. The variations of the h_d values for the hydraulic structures of rectangular and parabolic weirs are approximately the same, and their values are greater than those for the hydraulic structures of triangular weirs. For clarification, the actual discharge through the triangular weir is the smallest one compared with the other weir shapes for the same water depth over the weir crest, and this status will be reflected directly on the water depth downstream.

The variation of the Q_{act} values against the D_p values is shown in Figure 6, considering hydraulic structures of different weir shapes with pier-collar systems of D_r and te equal to 5cm and 0.5cm, respectively. It can be seen from the figure that the Q_{act} values decrease with increasing D_p values. Increasing the D_p values leads to the confinement of a large quantity of the flowing water in the upstream region of the pier-collar system, which in turn causes a decrease in the Q_{act} values. The variations of the Q_{act} values for the hydraulic structure of a triangular weir are less than those for the hydraulic structures of the other weir shapes.

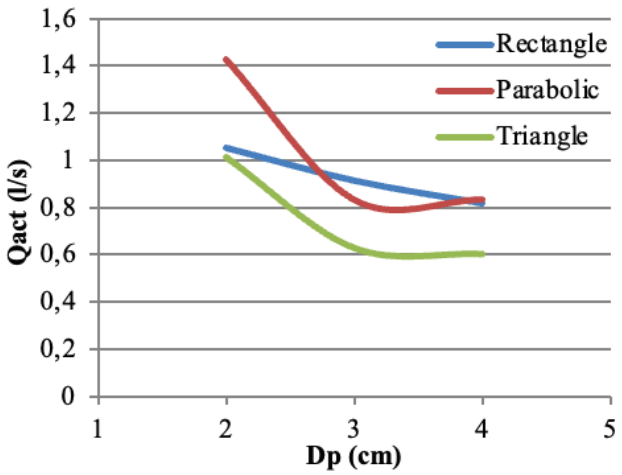

Figure 6. Q_{act} versus D_p for composite structures of different weir shapes (D_r=5 cm, te=0.5 cm).

Figure 7 shows the relationship between the h_d and D_p values for the same arrangement of the composite structures and pier-collar system indicated in Figure 6. In general, as the D_p value increases, the confinement to the flow increases, which in turn causes a reduction in flow velocity and an increase in the water depth value (h_d). This situation is clearly shown for the composite structure of the rectangular weir, whereas it is only slightly shown for the composite structures of the other weir shapes.

The influence of the D_p values on the change of momentum at the pier-collar system for the same arrangement of the composite structures and pier-collar system indicated in Figure 6 was presented in Figure 8. It is obvious from the figure that the change in momentum value increases with an increase in the D_p value. The change in momentum is described by a difference between the drag and static forces, where the former are exerted by the pier-collar system whereas the latter are produced by the static pressure. When the pier diameter increases, this leads to an increase in the projection area of the pier; therefore, the drag force and static force will increase simultaneously, taking into consideration that both forces depend on the projection area of the pier, so as a result, the moment will increase directly. Also, the drag force, which is produced and developed by the collar, has a direct effect on the value of the moment change.

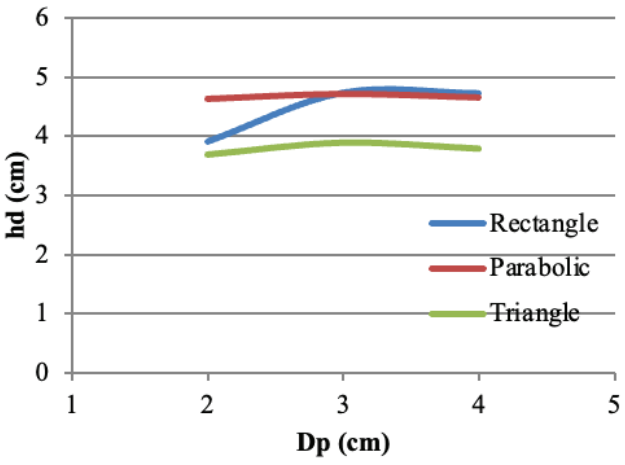

Figure 7. h_d versus D_p for composite structures of different weir shapes (D_r=5 cm, te=0.5 cm).

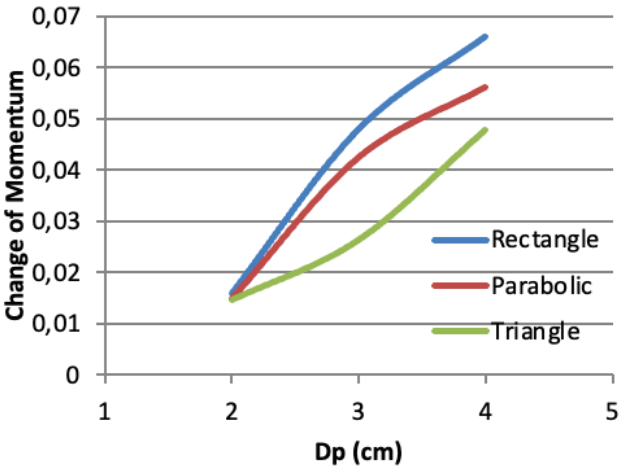

Figure 8. Variation of change of momentum with D_p value for composite structures of different weir shapes (D_r=5 cm, te=0.5 cm).

Figure 9 illustrates the variation of downstream Froude number (Fr_{down}) and R_n values at the downstream region of the composite structure with dimensionless values of the pier diameter (D_p/B) for a composite structure of a rectangular weir with a pier-collar system of D_r and te values equal to 5cm and 0.5cm, respectively. The Fr_{down} and R_n values were determined based on an average value of h_d (h_{davg}). As the (D_p/B) value increased, the values of Fr_{down} and R_n decreased monotonically, as shown in Figure 9. As indicated in Figures 6 and 7, the Q_{act} and h_d values decreased with increasing D_p values. Therefore, with increasing in h_d values, the Fr down value decreased due to the inverse relationship between Fr and water depth (eq. 12). Also with a decrease in Qact value, R_n decreased due to the direct proportionality between R_n and water flow rate (eq. 11).

Figure 10 illustrates the variations of Fr_{down} and R_n values at the downstream region of the composite structure with dimensionless values of the collar diameter (D_r/B) for the composite structure of a rectangular weir with a pier-collar system of D_p and te values equal to 2cm and 0.5cm, respectively. As shown in the figure, as the (D_r/B) increases, both the Froude number and the Reynolds number increase.

As indicated in Figure 4, the h_d value increased with increasing D_r values. Therefore, with increasing in h_d values, the Fr down value decreased due to the inverse relationship between Fr and water depth (eq. 12). The diameter of the collar is very small as compared with the water depth, so the collar diameter has a minor effect on the result of the Froude number and Reynolds number. Here, the results remain affected by the water depth for the Froude number and the flow velocity for the Reynolds number. Any variation in the result will be attributed to the interaction between overflow velocity and underflow velocity.

Figure 11 illustrates the variation of Fr_{down} and R_n values at the downstream region of the composite structure with dimensionless values of the collar depth (te/B) for a composite structure of a rectangular weir with a pier-collar system of D_p and D_r values equal to 2cm and 5cm, respectively. The value of the Fr_{down} decreased monotonically with increasing (te/B) values, whereas the R_n values increased and then decreased with increasing (te/B) values (Fig. 11). Increasing the te value provides additional confinement to the flow, which causes an increase in water depth and then a decrease in the Fr_{down} value (eq. 12). Also, the figure shows a dramatic relationship between the Reynolds number and (te/B); this happens due to the alteration in the flow velocity behavior and the change in the water depth around the pier, which is mounted with a collar.

Figure 12 shows the variation of the Q_{act} value with the C_d value for composite structures of different weir shapes

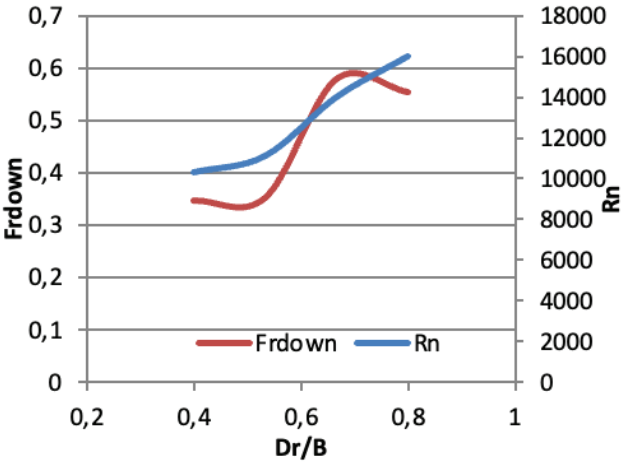

Figure 10. Variation of Fr_{down} and R_n with dimensionless value of D_r for composite structure of rectangular weir (D_p=2 cm, te=0.5 cm).

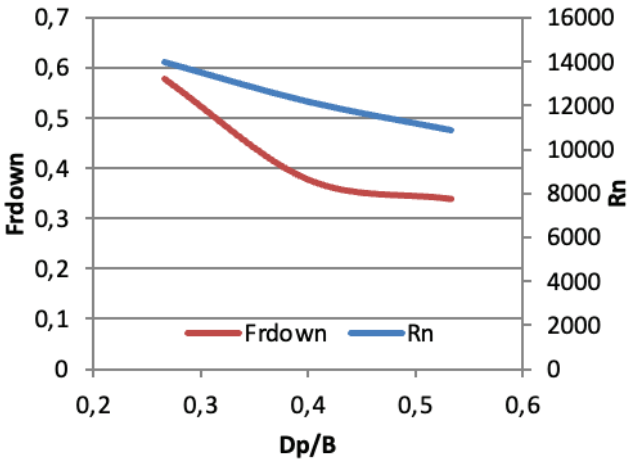

Figure 9. Variation of Fr_{down} and R_n with dimensionless value of D_p for composite structure of rectangular weir (D_r=5 cm, te=0.5 cm).

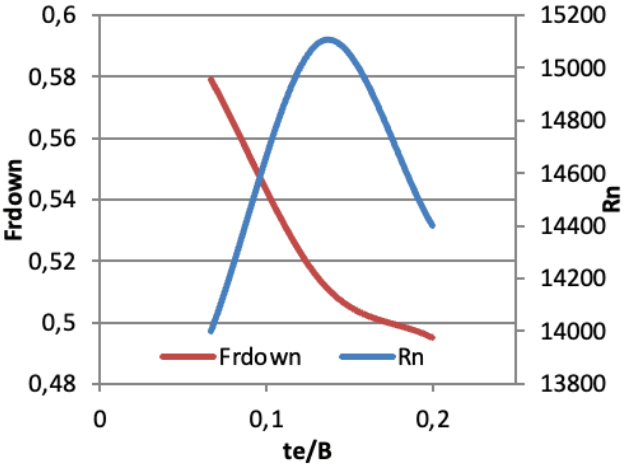

Figure 11. Variation of Fr_{down} and R_n with dimensionless value of te for composite structure of rectangular weir (D_p=2 cm, D_r=5 cm).

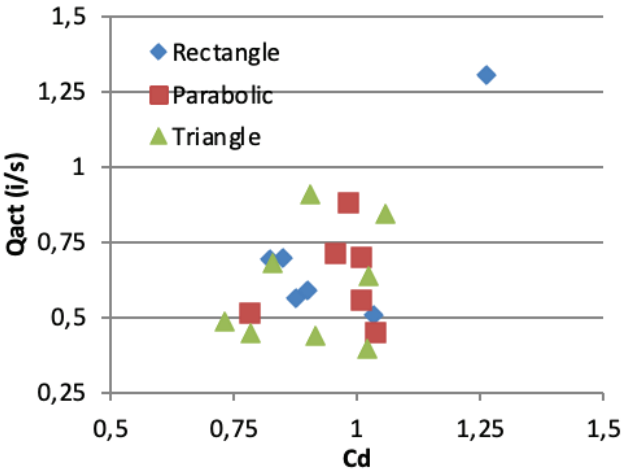

Figure 12. Variation of Q_{act} with C_d for composite structures of different weir shapes (D_p=3 cm, D_r=4 cm, te=1cm).

with pier-collar systems of the D_p, D_r, and te values equal to 3 cm, 4 cm, and 1 cm, respectively. It is obvious from the figure that the Q_{act} value increases with an increase in the C_d value, and this is due to the direct proportionality between them.

Figure 13 illustrates the variation of the variable (H_{new}) and the upstream Froude number (Fr_{up}) for the same arrangement of the composite structures and pier-collar system indicated in Figure 12. The figure shows that the value of Fr_{up} increases with increasing H_{new} values for all shapes of the composite structures, and this is due to the direct proportionality between Froude number and flow depth.

Figures 14 (a), (b), (c), (d), and (e) show the variations of the average value of $h_{d\ average}$ with pier C_D, F_D (pier), F_D (collar), and F_p at the upstream and downstream regions of the pier for composite structures of different weir shapes

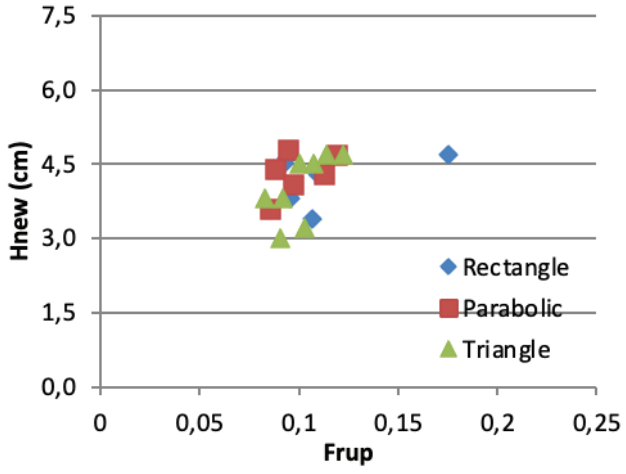

Figure 13. Variation of H_{new} with Fr_{up} for composite structures of different weir shapes (D_p=3 cm, D_r=4 cm, te=1cm).

with pier-collar systems of the D_p, D_r, and te values equal to 4cm, 5cm, and 1cm, respectively. It is clear from the above figures that any increase in the $h_{d\ average}$ will be reflected directly in the mentioned values. In general, the water depth has a direct effect on the drag force value (eq. 13) and on the R_n value, which dominates the value of C_D (eq. 14). In addition, the $h_{d\ average}$ value has a direct impact on the calculated values of the static force due to the direct proportionality between them (eq. 15).

The relationship of the Q_{act} and D_P values for the composite hydraulic structure of a rectangular weir-ellipse gate with a collar of different D_r values and te value of 0.5cm is shown in Table 2. For a constant D_p value, the Q_{act} value increases with an increase in the D_r value. Also, for a constant D_r value, the Q_{act} value fluctuates with an increase in the D_p value due to the interaction between weir discharge and gate discharge.

The relationship between the F_{rdown} and D_P values for the same arrangement indicated in Table 2 is shown in Table 3. For a constant D_p or D_r value, the Q_{act} value increases with an increase in the D_r or D_p value, respectively.

The relationship between the h_d and D_P values for the same arrangement indicated in Table 2 is shown in Table 4. For a constant D_p value, the h_d value increases with an increase in the D_r value, except for the case when D_p = 2 cm, where the h_d values decrease and then increase when the D_r values change from 4cm to 5cm and from 5cm to 6cm, respectively. Also, for a constant h_d value, the Q_{act} value fluctuates with an increase in the D_p value due to the weir flow velocity and gate flow velocity.

The relationship between the change in momentum and D_P values for the same arrangement indicated in Table 2 is shown in Table 5. The variation in the change of momentum values was clearly shown, and it depends mainly on the size of the pier and collar and also on the interference between weir and gate flow velocities, respectively.

The relationship of the Q_{act} and D_P values for the composite hydraulic structure of a rectangular weir-ellipse gate with a collar of different te values and D_r value of 5cm is shown in Table 6. For constant D_p value, the Q_{act} value is fluctuated with increasing in the te value due to the interaction between weir discharge and gate discharge. For a constant te value, the Q_{act} value decreases with increasing in the D_p value except for the case when te = 1.5 cm, where the Q_{act} values have increased and then decreased when the

Table 2. Q_{act} versus D_p for rectangular weir-ellipse gate composite structure with different D_r values (te=0.5cm)

D_p (cm)	Q_{act} (l/sec)		
	D_r=4cm	D_r=5cm	D_r=6cm
2	0.829	1.052	1.201
3	0.831	0.914	1.424
4		0.818	0.**783**

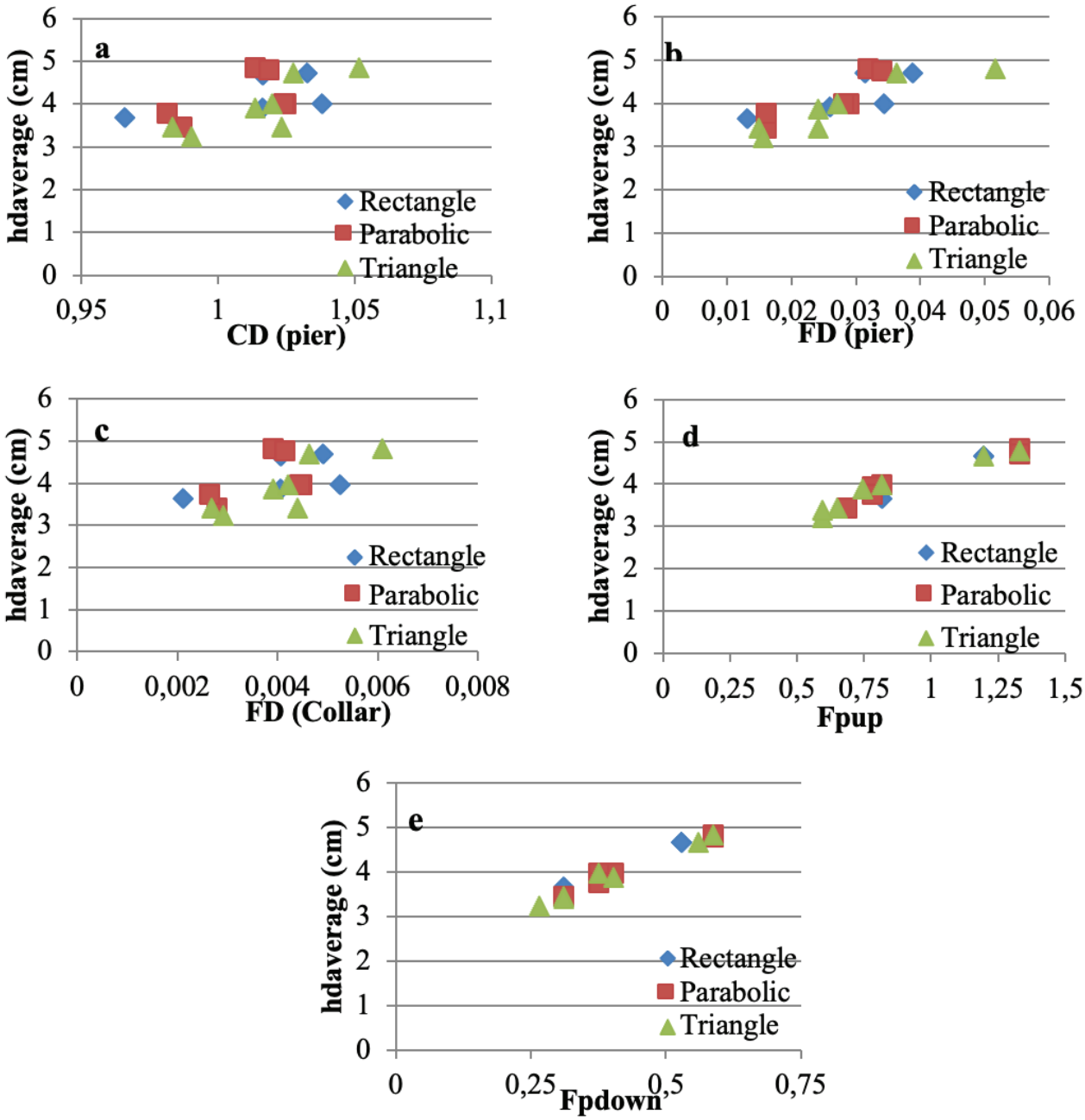

Figure 14. Variations of the $h_{daverage}$ with; (a) C_D(pier) , (b) F_D(pier), (c) F_D(collar) , (d) F_{Pup} , and (e) F_{Pdown} for composite structures of different weir shapes (D_p=4 cm, D_r=5 cm, te=1cm).

Table 3. F_{rdown} versus D_p for rectangular weir-ellipse gate composite structure with different D_r values (te=0.5cm)

D_p (cm)	F_{rdown}		
	D_r=4cm	D_r=5cm	D_r=6cm
2	0.353	0.579	0.554
3	0.395	0.377	0.554
4		0.338	0.365

Table 4. h_d versus D_p for rectangular weir-ellipse gate composite structure with different D_r values (te=0.5cm)

D_p (cm)	h_d (cm)		
	D_r=4cm	D_r=5cm	D_r=6cm
2	4.64	3.19	4.40
3	4.31	4.74	4.93
4		4.73	4.37

Table 5. Change of momentum versus D_p for rectangular weir-ellipse gate composite structure with different D_r values (te=0.5cm)

D_p (cm)	Change of momentum (N)		
	D_r=4cm	D_r=5cm	D_r=6cm
2	0.0369	0.016	0.0428
3	0.0256	0.049	0.0172
4		0.0664	0.0638

Table 6. Q_{act} versus D_p for rectangular weir-ellipse gate composite structure with different te values (D_r=5cm)

D_p (cm)	Q_{act} (l/sec)		
	te=0.5cm	te=1cm	te=1.5cm
2	1.053	1.129	1.079
3	0.914	0.937	1.163
4	0.817	0.703	0.824

Table 7. Fr versus D_p for rectangular weir-ellipse gate composite structure with different te values (D_r=5cm)

D_p (cm)	F_{rdown}		
	te=0.5cm	te=1cm	te=1.5cm
2	0.579	0.320	0.306
3	0.377	0.297	0.304
4	0.338	0.246	0.281

Table 8. h_d versus D_p for rectangular weir-ellipse gate composite structure with different te values (D_r=5cm)

D_p (cm)	h_d (cm)		
	te=0.5cm	te=1cm	te=1.5cm
2	3.91	4.44	4.41
3	4.74	4.71	4.59
4	4.73	4.69	4.56

Table 9. Change of momentum versus D_p for rectangular weir-ellipse gate composite structure with different te values (D_r=5cm)

D_p	Change of Momentum (N)		
(cm)	te=0.5cm	te=1cm	te=1.5cm
2	0.016	0.0217	0.037
3	0.048	0.066	0.026
4	0.066	0.058	0.051

D_p values have changed from 2cm to 3cm and from 3cm to 4cm, respectively.

The relationship between the F_{rdown} and D_p values for the same arrangement indicated in Table 6 is shown in Table 7. For a constant D_p value, the F_{rdown} value fluctuates with an increase in the te value. For constant te the Fr value decreases with an increase in the D_p value.

The relationship between the h_d and D_p values for the same arrangement indicated in Table 6 is shown in Table 8. For a constant D_p or te value, the h_d value fluctuates with an increase in the te or D_p value, respectively. These fluctuations in the h_d values were attributed to the interaction between weir flow velocity and gate flow velocity.

The relationship between the change in momentum and D_p values for the same arrangement indicated in Table 6 is shown in Table 9. The variation in the change of momentum values was clearly shown, and it depends mainly on the size of the pier and collar and also on the interference between weir and gate flow velocities, respectively.

To examine the impact of pier-collar systems on the weir-gate structure, it has been considered how these systems affect the primary hydraulic and geometrical variables that control the hydraulic function of the weir-gate structure. These variables include the water depth of the weir, the vertical distance between the weir and the gate, and the water depth of the gate. Figure (15) displays the variation in the weir water depth with the Froude number for the hydraulic regime for the case, te=1cm, y=4cm, d=3cm, D_p=4cm, and D_r=6cm for three different shapes of weir (rectangular, triangular, and parabolic), based on the alteration in the pier drag force, collar drag force, and hydrostatic pressure at the upstream and downstream faces of the pier. It has been inferred from the figure that rectangular and parabolic weirs respectively, with an increase in the water depth above the weir crest, the Froude number increases directly.

Here, the Froude number depends on the downstream flow velocity and downstream water depth, the downstream water depth relies on the hu, y, and d. If the summation of both values of hu and d is checked, it is found that the summation is always greater than y. Therefore, when the downstream water depth (hu+d) becomes greater than y, the Froude number must decrease directly owing to the inverse proportional between them despite of rise in hu values. Still the interference between weir flow velocity and gate flow velocity will share directly in the increases in Froude number values, owing to the direct proportionality between flow velocity and Froude number. Here, y confine the water depth behind the weir-gate structure. Furthermore, for any curve in the figure, the upstream and downstream hydrostatic pressure increase directly owing to the hydrostatic pressure being directly proportional to the water depth near the pier. Therefore, the rise in water depth leads to a rise in hydrostatic pressure, while the drag force has a linear trend because the water depth rise has a minor impact on the drag force as compared with flow velocity. For a triangular weir,

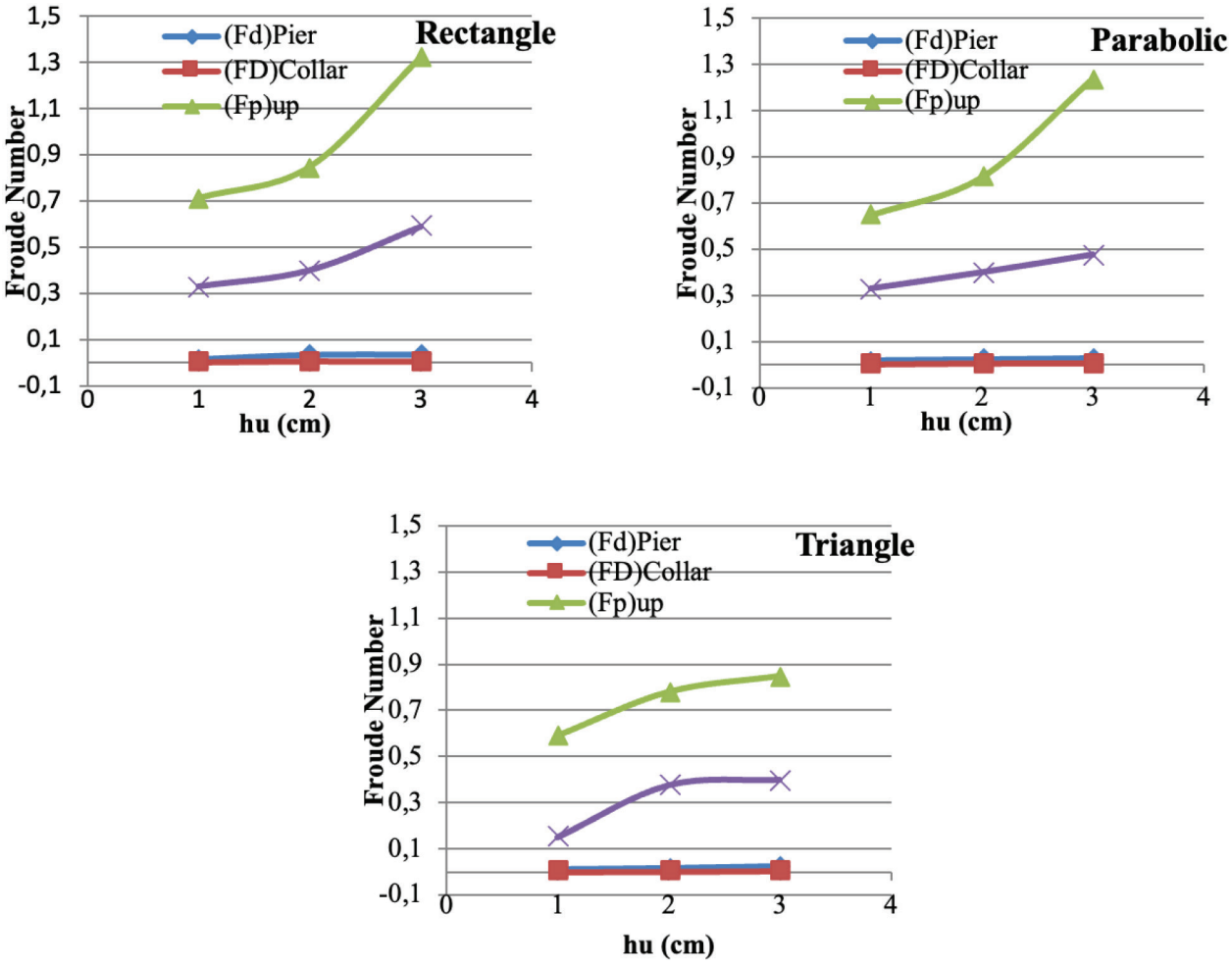

Figure 15. Variation of hu with Froude Number of hydraulic regime for the case, te=1cm, y=4cm, d=3cm, D_p=4cm, and D_r=6cm

there are slightly changes in the relationship trend between water depth over the weir and Froude number, and this occurs owing to the interaction between the weir and gate flow velocity.

The alteration in the Froude number with the water depth above the rectangular weir crest is plotted in Figure 16, considering the variation in the drag force of pier and collar, respectively, for different values of (y). Also, the variation in the (y) values leads to a variation in the values of (d). Two different values are adopted for (y), and these values are y = 4 cm and y = 4.5 cm. It is clear from the figure that with an increase in the water depth above the weir crest, the pier drag force and collar drag force increase sharply. Here, the increase in the hu values leads to an increase in the project area of the pier which has direct contact with water. As the projection area increases the drag force will be increase due to the direct proportionality between drag force and projection area. Also, the alteration in the Froude number with the water depth above the rectangular weir crest is plotted in Figure 16, considering the variation in the upstream and downstream hydrostatic pressure, respectively, for different values of (y). Also, the variation in the (y) values leads to a variation in (d) values. Two different values are adopted for (y) and these values are y = 4cm and y = 4.5cm. It is clear from the figure that with an increase in water depth above the weir crest, the Froude number increases directly. Here, the Froude number depends on the downstream flow velocity and downstream water depth, the downstream water depth relies on the hu, y, and d. It is found that the summation of both values of hu and d is always greater than y. Therefore, when the downstream water depth (hu+d) becomes greater than y, the Froude number must decrease directly owing to the inverse proportionality between them despite the rise in hu values, but the interference between weir flow velocity and gate flow velocity will share directly in the increase of Froude number values, owing to the direct proportionality between flow velocity and the Froude number. Here, y confine the water depth behind the weir-gate structure.

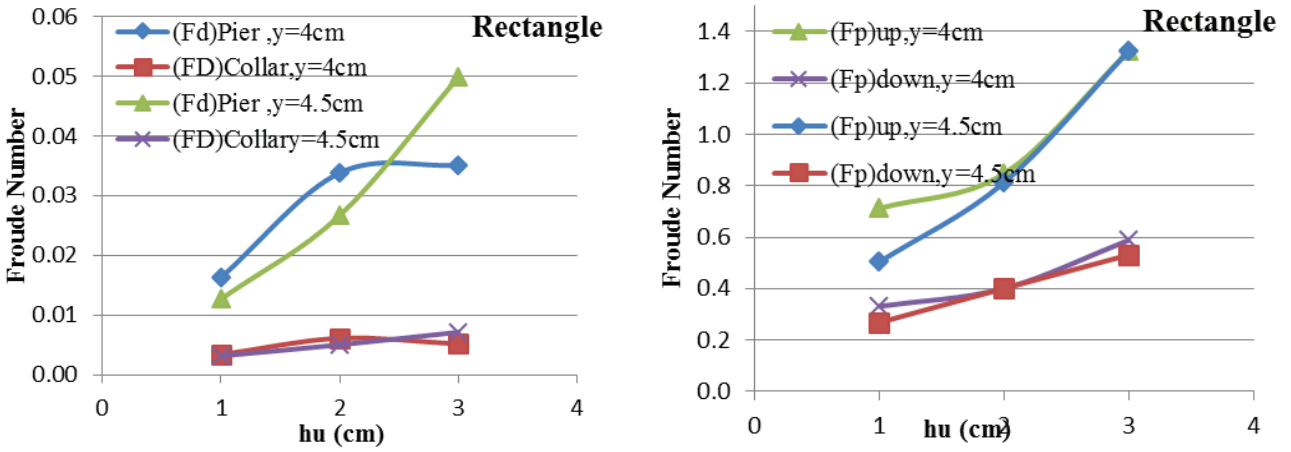

Figure 16. Variation of Froude Number with y and d for the case, te=1cm, H=9cm, Dp=4cm, and D_r=6cm.

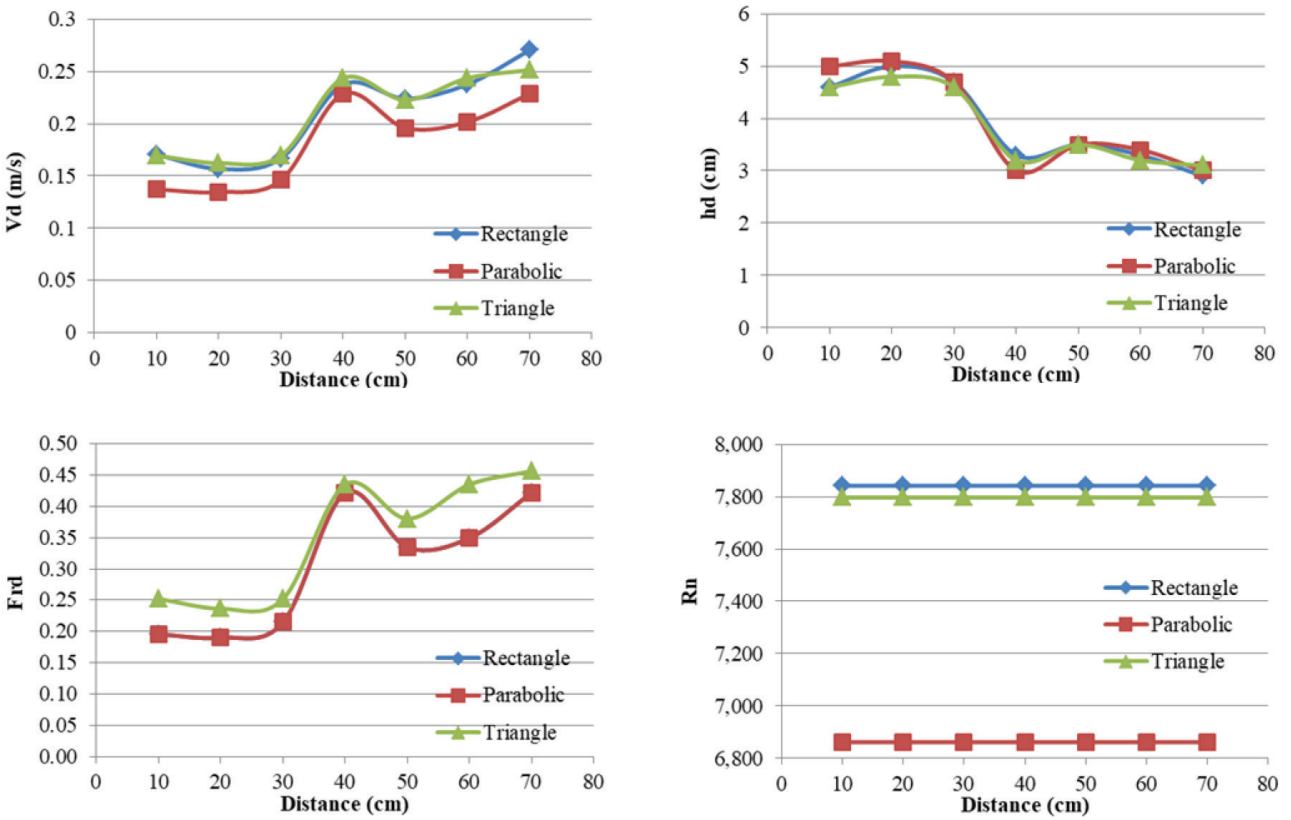

Figure 17. The Profile of downstream velocity, water depth, Froude Number, and Reynold's Number for the case te=1cm, y=4cm, d=3cm, D_p=4cm, and D_r=6cm.

To show the hydraulic patterns due to the interaction between the pier-collar system and the weir-gate structure the alteration in flow velocity, flow depth, Froude numbers, and Reynolds numbers with distance has been plotted respectively using three different weir shapes (rectangular, triangular, and parabolic). Commonly, both Froude number and Reynold's number depend on the flow velocity and flow depth. Figure 17 shows subcritical and turbulent open channel flow. The Froude number profile is similar to the velocity profile owing to the direct proportion between them. Any variation in hydraulic trend will be attributed to flow depth, which is inversely proportional to the Froude

number, and the overlapping between over weir flow and under gate flow will be shared in the flow velocity variation, which will be reflected directly on the Froude number or Reynolds number. The trend in relation between Reynolds numbers and distance is described as linear, regardless of the weir shapes.

QUANTIFYING STATE VARIABLE UNCERTAINTY INTERVALS

The best data available must be utilized to estimate the systematic and random errors. Equation (17) is employed to compute the random error S_x. Then, $(=S_x/\sqrt{N})$ is the standard uncertainty of the mean $S_{\bar{x}}$. Systematic uncertainty estimates cannot be obtained typically from measurements or statistical processes. The elemental error sources that impact each measurement are the first thing to take into account when estimating the systematic uncertainty for a particular variable.

Table 10 shows the potential sources of the two variables (actual discharge and average downstream water depth) that will be assessed in this experiment.

Table 10. Elemental systematic uncertainty details

Source	Systematic uncertainty	
	Actual discharge (l/s)	Downstream water depth (cm)
Conceptual	0.073	0.212
Calibration	0.012	0.100
Calibration	0.006	0.200

The evaluation of systematic uncertainty is based on potential sources of inaccuracy. Conceptual errors are a major source of errors in the composite structure computation experiment. This form of inaccuracy occurs when the measured values at certain sites diverge from the mean value. Table 11 shows the actual discharge values, averaged over three tries, as well as the percentage variance between the values and their average. Table 12 also displays the downstream water depth readings for various locations, the average of these values, and the percentage difference between the average and these values. The absolute average

Table 11. Selected values of actual discharge and differences

Q1 (1)	Q2 (2)	Q3 (3)	Qact (4)	D1= $[\frac{(1)-(4)}{(4)}]$	D2= $[\frac{(2)-(4)}{(4)}]$	D3= $[\frac{(3)-(4)}{(4)}]$
0.6067	0.5946	0.5325	0.5760	0.053	0.032	-0.076
0.5606	0.5653	0.4693	0.5278	0.062	0.071	-0.111
0.6385	0.5693	0.5412	0.5802	0.100	-0.019	-0.067
0.5869	0.5988	0.5948	0.5935	-0.011	0.009	0.002
0.6610	0.6063	0.5553	0.6045	0.094	0.003	-0.081
0.6397	0.6742	0.5357	0.6106	0.048	0.104	-0.123
0.6116	0.5581	0.5556	0.5740	0.066	-0.028	-0.032
0.5784	0.5291	0.4835	0.5275	0.097	0.003	-0.083
0.6106	0.5357	0.6572	0.5969	0.023	-0.102	0.101

Table 12. Selected of average downstream water depth and differences

hd1	hd2	hd3	hd4	hd5	hd6	hd7	hdavg	D1	D2	D3	D4	D5	D6	D7
4.2	4.5	3.8	3.7	3.2	3.0	2.6	3.57	0.176	0.26	0.064	0.036	-0.104	-0.16	-0.272
4.4	4.6	4.3	3.8	4.0	3.7	3.5	4.04	0.088	0.138	0.064	-0.060	-0.011	-0.085	-0.134
4.3	4.5	4.3	3.7	3.7	3.7	3.5	3.96	0.087	0.137	0.087	-0.065	-0.065	-0.065	-0.116
4.5	5.0	4.8	4.2	4.3	4.0	3.8	4.37	0.029	0.144	0.098	-0.039	-0.016	-0.085	-0.131
5.3	5.5	5.3	4.0	4.5	4.0	3.8	4.63	0.145	0.188	0.145	-0.136	-0.028	-0.136	-0.179
4.4	4.5	4.5	3.5	3.5	3.5	3.3	3.89	0.132	0.158	0.158	-0.099	-0.099	-0.099	-0.151
4.0	4.0	3.8	3.2	3.2	3.0	2.8	3.43	0.167	0.167	0.108	-0.067	-0.067	-0.125	-0.183
5.3	5.5	5.5	4.2	4.5	4.2	4.0	4.74	0.117	0.160	0.160	-0.114	-0.051	-0.114	-0.157
4.5	4.4	4.2	3.0	3.3	3.0	2.6	3.57	0.260	0.232	0.176	-0.160	-0.076	-0.160	-0.272

percentage difference of actual discharge and downstream water depth was calculated to be 0.229 and 0.106, respectively. Based on these values, the conceptual uncertainty value is considered to be 12% of the mean value of actual discharge and 5.3% of the mean value of average downstream water depth (about half the absolute average percentage variance). Thus, it can be computed by multiplying the percentage difference by the arithmetic mean of the actual discharge and the downstream depth of the water, respectively. It was found that these values were (0.12*0.609=0.073 l/s) and (0.053*4.013=0.212 cm).

The scalar readability was given a value of (0.1 cm), and the flow ripple in downstream was given a value of (0.2 cm), in relation to the uncertainty coming from the calibration and its connection to the downstream depth of the water. Also, in terms of calibration uncertainty and related to real discharge, the values (0.012 l/s) and (0.006 l/s) were assigned to errors caused by time estimation and other invisible errors, respectively. Table 13 shows the statistics of

Table 13. Statistics and uncertainty parameters of the state variables

Variable	Mean	*Sx*	$S_{\bar{x}}$	$b_{\bar{x}}$	*ux*	$U_{\bar{x}}$	Min.	Max.
Q_{act} (l/s)	0.609	0.168	0.0108	0.0913	0.0919	0.2391	0.3698	0.8481
hd_{avg} (cm)	4.013	0.506	0.0327	0.5127	0.5137	1.0270	2.986	5.0410

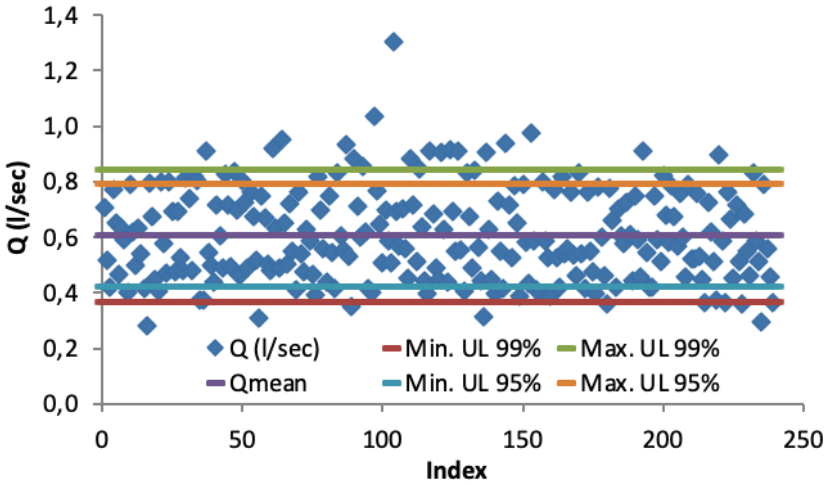

Figure 18. The actual discharge and its mean and uncertainty interval.

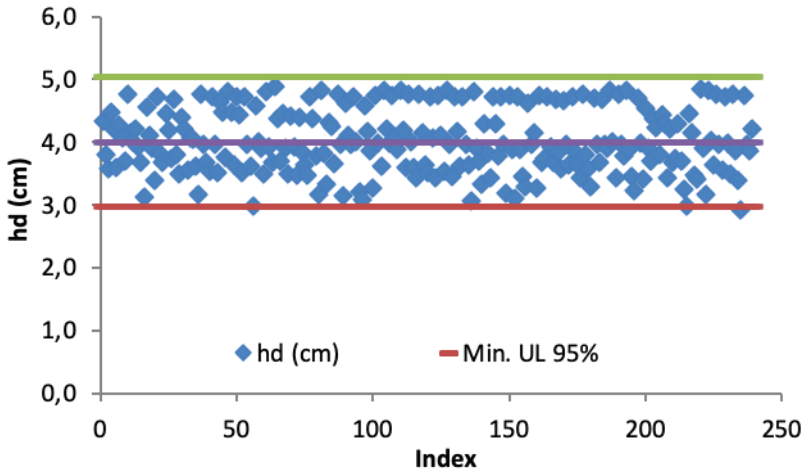

Figure 19. The downstream water depth and its mean and uncertainty interval.

the actual outflow and downstream water depth, as well as the components of uncertainty.

Figures 18 and 19 show plots of the data from Table 13. These graphs depict the mean as a solid line, the 99% and 95% uncertainty intervals for the true mean of the data for actual discharge, and the 95% uncertainty interval for downstream water depth. The uncertainty intervals cover 75% and 88% of the actual discharge values for 95% and 99% uncertainty intervals, respectively, and 100% of downstream water depth data for the 95% uncertainty interval. In this case, the greater variance of the actual discharge compared to the downstream water depth indicates that the experimental data for the actual discharge is more scattered or volatile. Coverage of 100% of the data for the downstream water depth within the uncertainty interval with a confidence level of 95% means that the data is less dispersed relative to the uncertainty interval. Coverage of 75% and 88% for the actual discharge with confidence levels of 95% and 99% reflects a significant increase in dispersion, which requires expanding the range of uncertainty to cover larger proportions of data.

CONCLUSION

The presence of a structure like a pier in the downstream region of the composite hydraulic structure will create a variation in the hydraulic characteristics and the response of the composite hydraulic structure. In addition to the alteration in the flow pattern along the reach of the flume, we can conclude the following vital points:

1. The average downstream water depth has a major impact on the calculated values of the developed moment, drag force, drag coefficient, and static force.
2. The alteration in the flow velocity has a direct impact on the values of the Froude number and Reynolds number.
3. The change in the flow of water depth due to the existence of the pier has a major effect on the values of the Froude number and Reynolds number.
4. The water flow velocity has a major impact on the calculated values of the developed moment, drag force, drag coefficient, and static force.
5. The collar structure has a moderate influence on the hydraulic characteristics of the composite hydraulic structure as compared with the presence of the pier structure.
6. The size of the pier and the collar have a noticeable impact on the values of the Froude number and the Reynolds number.
7. Pier diameter has a dramatic influence on the calculated values of actual discharge, downstream flow velocity, downstream water depth, and moment, which developed at the base of the pier.
8. The water surface profile downstream of the composite hydraulic structure can be described as nonlinear regardless of the pier diameter, collar diameter, and weir shape.
9. Weir shape plays a vital role in dominating the flow pattern between the pier and the composite hydraulic structure.
10. The error margins for actual discharge and downstream water depth are predicted to be 88% and 100% of the values, respectively. Furthermore, the best conclusion is that the downstream water depth is more consistent and dependable in its estimates than the actual discharge, which has a higher variance.

The novelty of the work has been concentrated on how the pier-collar system alter the hydrodynamic behavior and pattern at the downstream of combined structure, also the study deals with the hydraulic variables which has significant impact on the operation of combined structure owing to the pier-collar system, on the other hand the study contains investigation the effect of hydrodynamic response of pier-collar system.

The study limitations relied on several hydraulic and geometrical parameters. For hydraulic parameters, the dominant features are open channel flow regime patterns (flow type), water surface width, water depth before or after placing the weir-gate structure, flow velocity distribution downstream of the weir-gate before and after placing the structure, and flow losses. Geometrical parameters that share in the variation of the open channel or flume regime are pier size, collar size, and vertical distance between the weir and gate. Moreover, the naturality impact of the flume bed has a noticeable effect on flow pattern; in this study, the bed is considered rigid. Therefore, many experiments are done according to information available about the hydraulic features of the prototype channel to avoid any conflict among hydraulic parameters during the weir-gate hydraulic structure's serviceability life.

The implications of the study relied on the hydraulic interaction between flow at downstream of weir-gate structure with flow around pier mounted by collar, therefore to avoid this problem it should be maintained minimum water level or flow rate during hazard conditions like drying season.

It is recommended that before placing the weir-gate structure upstream of the pier in an open channel, many experiments must be done in the laboratory considering many variables that dominate the weir-gate hydraulic response, like weir water head, weir width, gate width, gate water depth, upstream weir-gate water depth, water surface width at upstream and downstream of weir-gate, the horizontal distance between weir-gate and pier, downstream water depth, pier size, and the location of the open channel inlet and outlet concerning both weir-gate and pier. After that, the obtained results were analyzed hydraulically and statistically in order to decide and choose a suitable case.

NOTATION

The following symbols are used in this paper:

H	*Upstream water level*

y	*Distance between top of gate and bottom of weir*
d	*Depth of gate*
b	*width of weir and gate*
B	*Total width of flume and/or composite structure*
h_d	*Downstream water depth*
A_g	*Area of gate*
A_w	*Area of weir*
$Q_{act.}$	*Measured discharge*
$Qw_{theo.}$	*Theoretical discharge through weir*
$Qg_{theo.}$	*Theoretical discharge through gate*
g	*Gravitational acceleration*
$ø$	*Weir angle*
f	*Focal distance*
hu	*Flow depth above weir crest*
Rn	*Reynold's number*
Fr	*Froude number*
V	*Flow velocity*
ρ	*Water density*
F_D	*Drag force*
Ap	*Pier or Collar projected area*
C_D	*Drag Coefficient*
Fp	*Hydrostatic force*
Dp	*Pier diameter*
C_d	*Discharge Coefficient*
H_{nwe}	*Difference between upstream and downstream water depth*
$hd_{average}$	*Average downstream water depth*
S_x	*Random errors*
b_x	*Systematic errors*
u_x	*The standard uncertainty .*
$U_{\bar{x}}$	*The expanded uncertainty*
N	*Number of measurements*
$\bar{x}$	*Mean Value*
$S_{\bar{x}}$	*The standard uncertainty of the mean*
$b_{\bar{x}}$	*The standard deviation associated with systematic errors*
k	*Coverage factor*

AUTHORSHIP CONTRIBUTIONS

Authors equally contributed to this work.

DATA AVAILABILITY STATEMENT

The authors confirm that the data that supports the findings of this study are available within the article. Raw data that support the finding of this study are available from the corresponding author, upon reasonable request.

CONFLICT OF INTEREST

The author declared no potential conflicts of interest with respect to the research, authorship, and/or publication of this article.

ETHICS

There are no ethical issues with the publication of this manuscript.

STATEMENT ON THE USE OF ARTIFICIAL INTELLIGENCE

Artificial intelligence was not used in the preparation of the article.

REFERENCES

[1] Qasim RM, Abdulhussein IA, Mohammed AA, Maatooq QA. Evaluation of the hydraulic behavior of the composite hydraulic structure considering a bed flume with special obstacle. INCAS Bull 2022;14:61–74. [CrossRef]

[2] Abdulhussein IA, Qasim RM, Mohammed AA, Maatooq QA. Flow-composite hydraulic structure-longitudinal obstacle interaction. Int J Geomate 2022;23:40–49. [CrossRef]

[3] Abdulhussein IA, Qasim RM, Maatooq QA. Hydraulic interaction between composite structure and block obstacle. Int J Tech Phys Probl Eng 2022;14:65–73.

[4] Qasim RM, Abdulhussein IA, Mohammed AA, Maatooq QA. The effect of the obstacle on the hydraulic response of the composite hydraulic structure. INCAS Bull 2020;12:159–172. [CrossRef]

[5] Qasim RM, Abdulhussein IA, AL-Asadi K. The effect of barrier on the hydraulic response of composite weir-gate structure. Arch Civ Eng 2020;66:98-118.

[6] Qasim RM, Mohammed AA, Abdulhussein IA, Maatooq QA. Experimental investigation of multi obstacles impact on weir-gate discharge structure. Int J Mechatron Appl Mech 2021;9:76–84.

[7] Abdulhussein IA, Qasim RM, Hameed MA. Determination of the general formula to estimate the discharge quantity of composite structure for free flow. Instrum Meas Metrol 2022;21:13–20. [CrossRef]

[8] Qasim RM, Abdulhussein IA, AL-Asadi K. Experimental study of composite inclined weir–gate hydraulic structure. WSEAS Trans Fluid Mech 2020;15:54–61. [CrossRef]

[9] Abdulhussein IA, Qasim RM, Al-Asadi K, Maatooq QA. The influence of weir crest on the hydraulic characteristics of a composite structure. Test Eng Manag 2020;83:24731–24743.

[10] Qasim RM, Mohammed AA, Abdulhussein IA. Review: weir–gate composite irrigation structure. Int J Eng Tech 2019;5:1–9.

[11] Qasim RM, Abdulhussein IA, Maatooq QA. Effect of bed flume contraction on discharge coefficient of composite weir-gate structure. Int J Sci Eng Investig 2019;8:40–45.

[12] Qasim RM, Abdulhussein IA, Hameed MA, Maatooq QA. Experimental study of coupled parabolic weir over flow and gate under flow rate. J Inf Eng Appl 2018;8:34–42.
[13] Qasim RM, Abdulhussein IA, Hameed MA, Maatooq QA. Experimental study of hydraulic response for combined weir-gate flow of composite shape. Civ Environ Res 2018;10:6–14.
[14] Qasim RM, Abdulhussein IA, Hameed MA. Analysis of flow over weir and under ellipse gate. Innov Syst Des Eng 2018;9:1–9.
[15] Qasim RM, Mohammed AA, Abdulhussein IA. An investigating of the impact of bed flume discordance on the weir-gate hydraulic structure. HighTech Innov J 2022;3:341-355. [CrossRef]
[16] Gharehbaghi A, Ghasemlounia R, Afaridegan E, Haghiabi A, Mandala V, Azamathulla HM, Parsaie A. A comparison of artificial intelligence approaches in predicting discharge coefficient of streamlined weirs. J Hydroinform 2023;25:1513. [CrossRef]
[17] Li S, Shen G, Parsaie A, Li G, Cao D. Discharge modeling and characteristic analysis of semi-circular side weir based on the soft computing method. J Hydroinform 2024;26:175-188. [CrossRef]
[18] Iqbal M, Ghani U. Prediction of the discharge capacity of piano key weirs using artificial neural networks. J Hydroinform 2024;26:175-188. [CrossRef]
[19] Kartal V, Emiroglu ME. Experimental analysis of combined side weir-gate located on a straight channel. Flow Meas Instrum 2022;88:102250. [CrossRef]
[20] Nouri M, Hemmati M. Discharge coefficient in the combined weir-gate structure. Flow Meas Instrum 2020;75:101780. [CrossRef]
[21] Streeter VL, Wylie EB. Fluid Mechanics. 1st SI Metric ed. New York: McGraw-Hill; 1983.
[22] Bos MG. Discharge Measurement Structures. 3rd ed. Int Inst Land Reclam Improv. The Netherlands: Wageningen; 1989.
[23] Fox RW, McDonald AT. Introduction to Fluid Mechanics. 4th SI ed. New York: John Wiley and Sons; 1994.
[24] Cheng NS. Calculation of drag coefficient for arrays of emergent circular cylinders with pseudo fluid model. J Hydraul Eng 2013;139:602–611. [CrossRef]
[25] Sharma MK, Sadhna AK, Bhargava, Kumar S, Rathour L, Mishra LN, Pandey S. A Fermatean fuzzy ranking function in optimization of intuitionistic fuzzy transportation problems. Adv Math Models Appl 2022;7:191–204.
[26] Sharma MK, Dhiman N, Kumar S, Rathour L, Mishra VN. Neutrosophic Monte Carlo simulation approach for decision making in medical diagnostic process under uncertain environment. Int J Neutrosophic Sci 2023;22:8–16. [CrossRef]
[27] Rathour L, Singh V, Yadav H, Sharma MK, Mishra VN. A dual hesitant fuzzy set theoretic approach in fuzzy reliability analysis of a fuzzy system. Inf Sci Lett 2024;13:433–440. [CrossRef]
[28] Chandola A, Pandey RM, Agarwal R, Rathour L, Mishra VN. On some properties and applications of the generalized m-parameter Mittag-Leffler function. Adv Math Models Appl 2022;7:130–145.
[29] Sharma MK, Chaudhary S, Rathour L, Mishra VN. Modified genetic algorithm with novel crossover and mutation operator in travelling salesman problem. Sigma J Eng Nat Sci 2024;42:1876-1883. [CrossRef]
[30] Negero NT, Duressa GF, Rathour L, Mishra VN. A novel fitted numerical scheme for singularly perturbed delay parabolic problems with two small parameters. Partial Differ Equ Appl Math 2023;8:1–8. [CrossRef]
[31] Hogeme MS, Woldaregay MM, Rathour L, Mishra VN. A stable numerical method for singularly perturbed Fredholm integro differential equation using exponentially fitted difference method. J Comput Appl Math 2024;441:115709. [CrossRef]
[32] Younus A, Dastgeer Z, Rathour L, Mishra LN, Mishra VN, Pandey S. Distinguishability criteria of conformable hybrid linear systems. Nonlinear Eng 2022;11:420–427. [CrossRef]
[33] Coleman HW, Steele WG. Experimentation, validation, and uncertainty analysis for engineers. 3rd ed. New York: Wiley; 2009. [CrossRef]
[34] JCGM 100: Evaluation of measurement data—Guide to the expression of uncertainty in measurement. GUM 1995 with minor corrections. Int Bureau of Weights and Measures (BIPM), Serres, France, 2008.